Molecular Biology of the Cell
Vol. 15, 5420–5430, December 2004

Rab9 GTPase Regulates Late Endosome Size and Requires Effector Interaction for Its Stability

Ian G. Ganley, Kate Carroll, Lenka Bittova, and Suzanne Pfeffer*

Department of Biochemistry, Stanford University School of Medicine, Stanford, CA 94305-5307

Submitted August 27, 2004; Revised September 15, 2004; Accepted September 16, 2004
Monitoring Editor: Jennifer Lippincott-Schwartz

Rab9 GTPase resides in a late endosome microdomain together with mannose 6-phosphate receptors (MPRs) and the tail-interacting protein of 47 kDa (TIP47). To explore the importance of Rab9 for microdomain establishment, we depleted the protein from cultured cells. Rab9 depletion decreased late endosome size and reduced the numbers of multilamellar and dense-tubule–containing late endosomes/lysosomes, but not multivesicular endosomes. The remaining late endosomes and lysosomes were more tightly clustered near the nucleus, implicating Rab9 in endosome localization. Cells displayed increased surface MPRs and lysosome-associated membrane protein 1. In addition, cells showed increased MPR synthesis in conjunction with MPR missorting to the lysosome. Surprisingly, Rab9 stability on late endosomes required interaction with TIP47. Rabs are thought of as independent, prenylated entities that reside either on membranes or in cytosol, bound to GDP dissociation inhibitor. These data show that Rab9 stability is strongly influenced by a specific effector interaction. Moreover, Rab9 and the proteins with which it interacts seem critical for the maintenance of specific late endocytic compartments and endosome/lysosome localization.

INTRODUCTION

Within the endocytic pathway, Rab GTPases serve to organize microdomains by recruiting specific sets of effector proteins to distinct regions (Zerial and McBride, 2001; Barbero *et al*., 2002; Miaczynska and Zerial, 2002). These collections of effector proteins act in concert to mediate specific endosomal functions such as endosome-endosome fusion, receptor segregation for recycling to the plasma membrane, or packaging of cargo into vesicles bound for another compartment. Zerial and coworkers have shown that early endosomes are comprised of at least three distinct domains containing Rab4, Rab5, or Rab11 (Sonnichsen *et al*., 2000).

Videomicroscopy of living cells revealed that Rab9 is segregated in a late endosome microdomain that is deficient in the late endosomal Rab7 GTPase (Barbero *et al*., 2002). The Rab9 microdomain contains mannose 6-phosphate receptors (MPRs; Barbero *et al*., 2002), which carry newly synthesized lysosomal enzymes from the Golgi complex to endosomes, and then return to the Golgi (Kornfeld, 1992). Two distinct MPRs have been identified, the ~46-kDa cation-dependent (CD) MPR and the ~300-kDa cation-independent (CI) MPR. Transport of MPRs from late endosomes to the *trans*-Golgi requires the Rab9 GTPase (Lombardi *et al*., 1993; Riederer *et al*., 1994), the cargo adaptor tail-interacting protein of 47 kDa (TIP47) (Diaz and Pfeffer, 1998; Carroll *et al*., 2001), a Rab9 effector named p40 (Diaz *et al*., 1997), NSF, α SNAP, and a protein named mapmodulin (Itin *et al*., 1997, 1999).

Article published online ahead of print. Mol. Biol. Cell 10.1091/mbc.E04–08–0747. Article and publication date are available at www.molbiolcell.org/cgi/doi/10.1091/mbc.E04–08–0747.

*Corresponding author. E-mail address: pfeffer@stanford.edu.

Abbreviations used: ESCRT, endosomal complex required for transport; GDI, GDP dissociation inhibitor; LAMP1, lysosome associated membrane protein 1; MPR, mannose 6-phosphate receptor; siRNA, small-interfering RNA; TIP47, tail-interacting protein of 47 kDa.

TIP47 binds with high specificity to the cytosolic domains of the CD-MPR and CI-MPR (Diaz and Pfeffer, 1998; Krise *et al*., 2000). TIP47 recognizes a Phe-Trp motif in the CD-MPR (Diaz and Pfeffer, 1998) and a proline-rich region of the CI-MPR (Orsel *et al*., 2000). In addition, TIP47 binds directly to Rab9, which enhances TIP47's affinity for MPR cytoplasmic domains (Carroll *et al*., 2001). In this way, Rab9 facilitates MPR cargo collection during the process of transport vesicle formation.

To explore further the role of Rab9 microdomains in late endosome function and to gain insight into interactions responsible for microdomain formation, we have taken a small-interfering RNA (siRNA) approach to deplete cells systematically of distinct microdomain constituents and then investigate the consequences. We show here that cells depleted of the Rab9 GTPase contain late endosomes that are smaller and fewer multilamellar and dense-tubule–containing structures. In addition, the stability of Rab9 is tightly regulated by TIP47 protein levels. These findings alter our thinking about the independence of Rab proteins on cellular membranes.

MATERIALS AND METHODS

Antibodies and Recombinant Proteins

His-tagged TIP47 was purified after expression in *Escherichia coli* as described previously (Diaz and Pfeffer, 1998). Recombinant Rab9CLLL was purified as described previously (Shapiro *et al*., 1993). Mouse and rabbit anti-Rab9 (Soldati *et al*., 1993), rabbit anti-Rab7 (Soldati *et al*., 1995), mouse and rabbit anti-CI-MPR (Lombardi *et al*., 1993; Dintzis *et al*., 1994), and rabbit anti-TIP47 (Diaz and Pfeffer, 1998) are previously characterized reagents. Lysosome-associated membrane protein 1 (LAMP1) monoclonal antibody H4A3 developed by J.T. August and J.E.K. Hildreth was obtained from the Developmental Studies Hybridoma Bank (Iowa City, IA) developed under the auspices of the National Institute of Child Health and Human Development and maintained by the Department of Biological Sciences (University of Iowa, Iowa City, IA). Alexa-488–conjugated goat anti-mouse and Alexa-594–conjugated goat anti-rabbit were from Molecular Probes (Invitrogen, Carlsbad, CA).

Cell Culture

HeLa and HeLaS3 cells from American Type Culture Collection (Manassas, VA) were cultured at 37°C and 5% CO_2 in DMEM supplemented with 7.5% fetal calf serum, penicillin, and streptomycin. For RNA interference, HeLa and HeLaS3 cells were transfected at 50% confluence with duplex RNA (Dharmacon Research, Lafayette, CO) by using Oligofectamine (Invitrogen) according to the manufacturer and analyzed 72 h posttransfection. Transfection efficiencies, determined by immunofluorescence and immunoblotting, were consistently in the range of 90%. TIP47 was targeted with the sequence AACAGAGCUACUUCGUACGUC and Rab9 with the sequence AAGUUUGAUACCCAGCUCUUC. The GL2 luciferase and lamin A/C control siRNAs have been described previously (Elbashir *et al*., 2001). Specific silencing of targeted genes was confirmed by at least three independent experiments.

Immunoblot Analysis

Cells were washed three times in phosphate-buffered saline (PBS) and then lysed at 4°C in radioimmunoprecipitation assay (RIPA) buffer (Dintzis *et al*., 1994) containing protease inhibitors for 20 min. Lysates were then collected by scraping with a rubber policeman and centrifuged for 15 min at 55,000 rpm at 4°C. Equal amounts of lysate protein were analyzed by immunoblot with enhanced chemiluminescence detection. Blots were quantified using ImageJ (National Institutes of Health, Bethesda, MD).

Immunofluorescence Microscopy

Cells were grown and transfected on glass coverslips. Cells were washed twice in PBS and then fixed for 20 min in 3.7% formaldehyde in 200 mM HEPES, pH 7.4. After fixing, cells were washed twice and incubated for 15 min in DMEM, 10 mM HEPES, pH 7.4, to quench the formaldehyde. Cells were then permeabilized for 5 min with 0.2% Triton X-100 in PBS. Free protein sites were blocked by washing twice and incubating for 15 min with 1% bovine serum albumin (BSA) in PBS. Cells were incubated with primary antibody, diluted in BSA/PBS, for 30 min followed by washes, and a 30-min incubation in secondary antibody diluted 1:1000 in BSA/PBS. After washes and mounting of coverslips, cells were imaged using a Zeiss Axiophot microscope fitted with a 40 and 63× lens and a cooled charge-coupled device (CCD) camera (NDE/CCD; Princeton Scientific Instruments, Monmouth Junction, NJ). Pictures were analyzed using MetaMorph (Universal Imaging, Downingtown, PA) and Adobe Photoshop (Adobe Systems, Mountain View, CA) software. All images were processed such that fluorescence levels within a figure could be compared quantitatively from each image to the next.

Antibody Internalization Assay

HeLa cells were grown and transfected on glass coverslips. Seventy-two hours posttransfection, cells were incubated in DMEM containing 30 μg/ml 2g11 monoclonal anti-CI-MPR or 30 μg/ml H4A3 monoclonal anti-LAMP1 for 15 min at 37°C to only stain surface and newly internalized proteins. Cells were then washed five times in PBS and fixed and stained with goat anti-mouse Alexa-594 as described for immunofluorescence microscopy.

Whole-Mount Electron Microscopy

Whole-mount electron microscopy was performed as described previously (Stoorvogel *et al*., 1996). Briefly, cells were seeded on Formvar/carbon-coated gold grids 24 h posttransfection and incubated for an additional 48 h. Before processing cells were incubated for 1 h in media containing 5 mg/ml dialyzed horseradish peroxidase (HRP) or 30 μg/ml mouse anti-CI-MPR conjugated to HRP, washed three times, and chased for 1 h in media without HRP. Cells were then washed rapidly with PBS at 4°C and incubated in 3,3′-diaminobenzidine (DAB) buffer (Sigma-Fast DAB set; Sigma-Aldrich, St. Louis, MO) for 30 min. After DAB polymerization, soluble cytosolic proteins were removed by permeabilizing the cells with 0.5 mg/ml saponin. Cells were then fixed with 2% formaldehyde, 0.2% gluteraldehyde in 0.1 M phosphate buffer, pH 7.4. Cells were dehydrated in ethanol, critical point dried, and coated with a carbon film. The grids were examined using a Jeol 1230 transmission electron microscope at 80–120 kV. Images were taken with a Gatan digital camera and processed using DigitalMicrograph (Gatan, Pleasanton, CA). The diameters of 265 late endosomal structures were measured from 14 different luciferase siRNA-treated cells and 248 from 13 different Rab9 siRNA-treated cells from two independent experiments. Statistical significance was calculated using the Student's *t*-Test.

Immunoelectron Microscopy

A modified version of the preembedding labeling technique developed by Seaman (2004) was used. siRNA-transfected cells, grown on 12-mm glass coverslips, were washed once in cold PBS and then once with cold glutamate lysis buffer (25 mM HEPES, pH 7.4, 25 mM KCl, 2.5 mM Mg-acetate, 5 mM EGTA, 150 mM K-glutamate). Coverslips were drained of excess buffer and cells were then snap frozen by immersing the coverslip in liquid nitrogen followed by thawing at room temperature for 60 s. Cells were washed twice in cold glutamate lysis buffer and then fixed at room temperature with 4% formaldehyde in 200 mM HEPES, pH 7.4 for 30 min, with one change of fixative after 10 min. After fixing, cells were washed twice and incubated for 10 min in DMEM, 10 mM HEPES, pH 7.4, followed by two washes and a 15-min incubation in 1% BSA in PBS. After these washes, cells were incubated for 30 min with mouse anti-Rab9 culture supernatant followed by a 30-min incubation with rabbit anti-Rab7 in BSA/PBS. After three washes in BSA/PBS cells were incubated for 30 min with 5-nm colloidal gold anti-mouse and 15-nm colloidal gold ant-rabbit, both diluted 1:50 in BSA/PBS. Cells were then fixed again in 2% formaldehyde, 2.5% glutaraldehyde in 200 mM HEPES, pH 7.4, for 1 h. Cells were postfixed in 1% OsO_4 and 1% uranyl acetate before being serially dehydrated in ethanol and embedded in epon. Glass coverslips were dissolved away for 15 min in HFl before sectioning. Sections were viewed and images taken as for the whole-mount samples.

Metabolic Labeling and Immunoprecipitation

Equal numbers of cells were split into 35-mm plates and grown overnight. Cells were transfected with the indicated siRNA and incubated for 24 h before labeling. For labeling, cells were washed twice with TD (Dintzis *et al*., 1994) and preincubated in methionine- and cysteine-free medium containing 7.5% dialyzed fetal calf serum for 30 min. Cells were then incubated for 1 h with 100 μCi of Tran[^{35}S]-label (MP Biomedicals, Irvine, CA), and then washed with media containing methionine and cysteine and chased for the indicated times. Cells were then transferred to ice, washed three times with PBS, and lysed in RIPA buffer containing protease inhibitors for 30 min. After centrifugation for 15 min at 55,000 rpm, the supernatant was precleared with RIPA-washed protein A-agarose. Proteins to be immunoprecipitated were incubated for 2 h at room temperature with 3 μl of polyclonal antibody. Immune complexes were isolated by 30-min incubation with protein A-agarose, washed four times in RIPA, and resuspended in SDS-sample buffer. Samples were separated by SDS-PAGE and analyzed by PhosphorImager for quantification (Amersham Biosciences, Piscataway, NJ).

Epidermal Growth Factor Receptor (EGFR) Down-Regulation

HeLa cells were transfected with Rab9, TIP47, or control (luciferase) siRNA. Seventy-two hours posttransfection, cells were serum starved for at least 5 h in DMEM supplemented with 0.5% BSA, penicillin, and streptomycin. Cells were chilled on ice and incubated for 10 min with 1.5 nM epidermal growth factor (EGF) (Sigma-Aldrich) in DMEM supplemented with 0.5% BSA and 10 mM HEPES, pH 7.4. Cells were then washed twice with ice-cold TD buffer, warmed up to 37°C for the indicated period of time, and harvested by scraping into RIPA buffer containing protease inhibitors. Cell lysates were centrifuged for 10 min at 200,000 × *g* at 4°C. Equal amounts of the clarified cell lysates (30 μg/lane) were resolved by SDS-PAGE and immunoblotted for EGFR and Rab9 or TIP47. EGFR was quantified using ImageJ software and plotted against time to obtain the rate of receptor down-regulation.

TIP47/Rab9 Binding Studies

Rab9 protein (100 nM) was allowed to bind radiolabeled GDP or GTPγS to equilibrium for 4 h at 37°C in the presence of TIP47 protein, added at the concentrations indicated (0–800 nM; Shapiro *et al*., 1993). The percent of Rab9 protein that can actively exchange nucleotide is increased upon the addition of recombinant TIP47 protein (Hanna *et al*., 2002). The stabilizing effect that TIP47 has for Rab9 nucleotide exchange is specific to TIP47 and is not seen with control proteins such as BSA or GFP (Hanna *et al*., 2002). Thus, increasing TIP47 concentrations in the nucleotide exchange assay are reflected by increasing amounts of radiolabeled nucleotide binding to Rab9. For ease of comparison, the data for the Rab9 binding to GDP and guanosine 5′-*O*-(3-thio)triphosphate (GTPγS) have been normalized and are plotted as fraction Rab9 bound to TIP47. Both nucleotide binding and TIP47 stabilization are complete at 4 h (Hanna *et al*., 2002).

Crude Membrane Fractionation

Control and TIP47 siRNA-transfected cells grown in 35-mm dishes were washed three times with PBS and once with 10 mM HEPES, pH 7.4, followed by a 15-min incubation at 4°C in 10 mM HEPES, pH 7.4, supplemented with protease inhibitors. Cells were harvested by scraping in homogenization buffer (20 mM HEPES, pH 7.4, 250 mM sucrose, 1 mM EDTA, 1 mM dithiothreitol plus protease inhibitors) and were homogenized with five passes through a 22-gauge needle. A postnuclear supernatant (PNS) was obtained by centrifugation of the homogenate at 3000 rpm at 4°C for 5 min. The PNS was further centrifuged at 98,000 rpm for 15 min at 4°C, and the supernatant (cytosolic fraction) was removed and the pellet (membrane fraction) was resuspended in a volume of homogenization buffer equal to that of the supernatant. Equal volumes of cytosol and membrane fractions were then subject to SDS-PAGE and immunblotting to determine the concentrations of membrane-bound and cytosolic TIP47 and Rab9.

RESULTS

We have shown previously that cells expressing a GDP-preferring Rab9 mutant protein (Rab9 S21N) display defects

in MPR transport from endosomes to the Golgi complex (Riederer *et al*., 1994). To investigate further the importance of Rab9 for the function and morphology of late endosomes, we used siRNA to deplete Rab9 from cultured cells. Immunoblot analysis showed that Rab9 protein was decreased >90% upon siRNA treatment (Figure 1A). The depletion seemed to be specific for Rab9 as the steady-state level of the late endosomal Rab7 protein was unchanged (Figure 1A). Loss of Rab9 did not alter the steady-state level of TIP47. This may not be surprising because the majority of TIP47 is cytosolic and that pool of TIP47 does not contain bound Rab9 (Diaz and Pfeffer, 1998). Similarly, the level of the late endosome/lysosomal marker LAMP1 increased only slightly upon Rab9 depletion (58%, Figure 1A; see below). However, loss of Rab9 led to a more significant increase in CI-MPR protein levels (Figure 1A).

The increase in CI-MPR levels was not due to a block in degradation: the MPR half-life decreased from 34 to 25 h, consistent with a small increase in MPR missorting to the lysosome (Figure 1B). Furthermore, careful examination of the levels of CI-MPRs detected at time 0 of this pulse-chase, protein biosynthesis experiment revealed a roughly 30% increase in CI-MPR protein biosynthesis rate. Over the 25 h half-life of the CI-MPR in cells lacking Rab9, we would therefore expect an increased accumulation of CI-MPRs that would be counterbalanced by the increase in degradation to yield a roughly twofold increase at steady state. Induction of MPR expression was seen previously in cells expressing Rab9 S21N (Riederer *et al*., 1994); cells expressing higher levels of MPRs can deliver newly synthesized lysosomal enzymes to the lysosome in the absence of MPR recycling.

The functionality of late endosomes depleted of Rab9 was analyzed by measuring the rate of EGF-stimulated EGF receptor degradation. This process is expected to be independent of Rab9 protein because it involves transport of EGF receptors to the lysosome. As shown in Figure 1C, the rate of EGF receptor degradation was unchanged in cells depleted of Rab9: EGF receptor half-life was close to 37 min in both control and depleted cells. Thus, Rab9 depletion does not seem to perturb endosome-to-lysosome transport.

We next examined the morphology of late endosomes in cells lacking Rab9 (Figure 2). In the absence of Rab9, Rab7 displayed a more restricted, perinuclear localization with an apparent reduction in the number of larger, peripheral vesicular structures compared with control cells (Figure 2A, bottom left and right). Similarly, LAMP1 staining revealed a reduction in larger, peripheral spherical structures accompanied by a much tighter perinuclear localization in Rab9-depleted cells (Figure 2B, left and right). The tighter perinuclear staining in the absence of Rab9 could be explained if Rab9 normally recruits a yet-to-be-identified motor protein involved in late endosome distribution. The LAMP1 distribution seemed to be more significantly concentrated than that of Rab7; this could be due to the presence of a portion of Rab7 on earlier compartments that do not contain Rab9. Alternatively, loss of Rab9 may lead to the release of a motor protein from late endosomes that is now available for clustering of LAMP1-positive lysosomes.

A possible reduction in the size of late endosomes in Rab9-depleted cells was explored further using whole-mount electron microscopy (Figure 3). Stoorvogel and coworkers have devised a method to grow cells directly on EM grids and to label endosomes selectively by endocytosis of HRP or conjugates thereof (Stoorvogel *et al*., 1996). Cells were incubated with HRP for 60 min at 37°C followed by a 30-min chase to fill late endosomes (and not lysosomes). Samples were then fixed, permeabilized, and visualized in

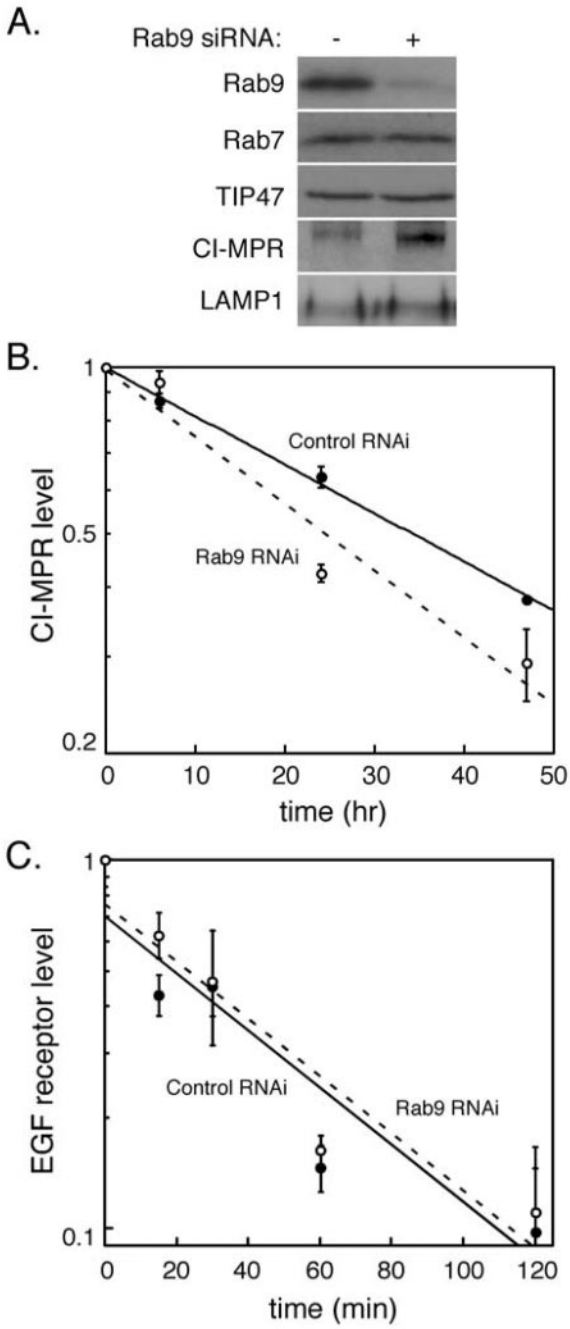

Figure 1. Rab9 depletion destabilizes CI-MPRs and induces their expression. (A) Immunoblot analysis of HeLa cell lysates (equal protein amounts) treated for 72 h with luciferase control siRNA (−) or Rab9 siRNA (+) by using the indicated antibodies. (B) HeLa cells, transfected with Rab9 or control siRNA, were pulse labeled with [^{35}S]methionine/cysteine and chased for the indicted times. Cells were then harvested and CI-MPR immunoprecipitated and quantified by autoradiography. Shown are the relative amounts of CI-MPR in control siRNA-treated samples (closed circles) and Rab9 siRNA-treated samples (open circles) over time from two independent experiments. Error bars represent SD. (C) HeLa cells, transfected with Rab9 or control siRNA, were incubated with EGF at 4°C and then shifted to 37°C for the indicated times to allow EGF receptor internalization and degradation. Cells were then harvested and the amount of EGF receptor in each sample was quantified by immunoblot. Shown are the relative amounts of EGF receptor in control siRNA-treated samples (closed circles) and Rab9 siRNA-treated samples (open circles) over time from four independent experiments. Error bars represent SE of the mean.

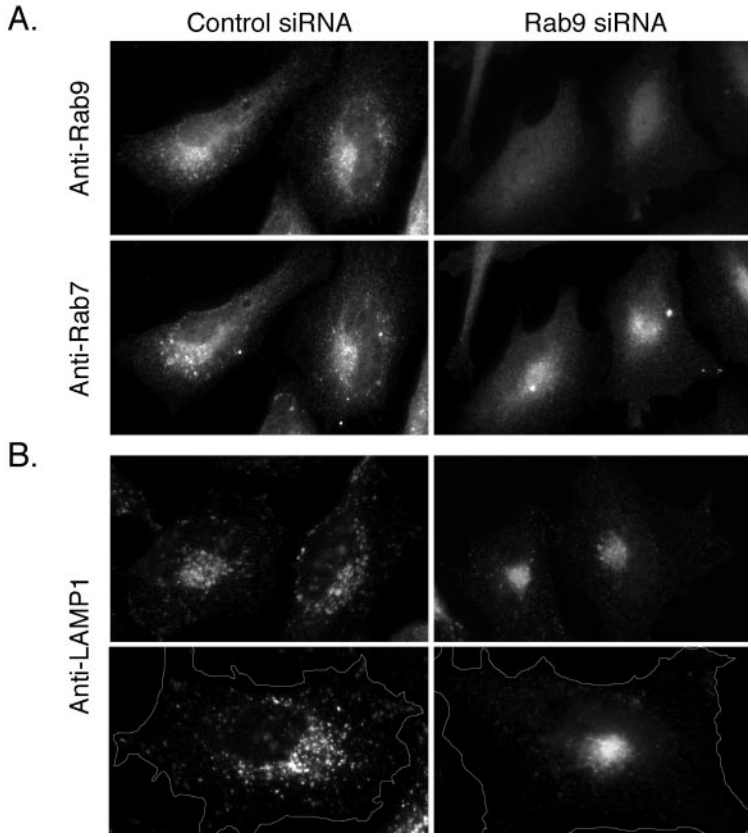

Figure 2. Late endosome morphology is altered in Rab9 depleted cells. (A) Immunofluorescence microscopy of HeLa cells transfected with control siRNA (left) or Rab9 siRNA (right) and double labeled with monoclonal anti-Rab9 antibody (top) or polyclonal anti-Rab7 antibody (bottom). (B) Control-transfected (left) or Rab9 siRNA-transfected (right) HeLa cells stained with monoclonal anti-LAMP1 antibody. The bottom panel pair is shown at higher magnification and outlined to highlight the distinction between control and depleted cells.

whole mount to view all late endosomes in both control and Rab9-depleted cells. Late endosomes look generally like perinuclear structures with vesicular and tubular elements (Stoorvogel *et al*., 1996; Kleijmeer *et al*. 2001; Figure 3A). Notably, in Rab9-depleted cells, late endosome diameters decreased by 45% ($p < 0.01$) from an average of 0.76 to 0.42 μm (Figure 3B). The cross-sectional area of individual late endosomes was decreased correspondingly ~70% ($p < 0.01$) from an average area of 0.37 to 0.11 μm^2 (Figure 3C). Thus, Rab9 knockdown reduces the size and volume of individual late endosomes.

We used conventional, thin-section electron microscopy to examine the structure of late endocytic compartments in HeLa cells treated with or without Rab9 siRNA (Figure 4). Three types of late endosomes/lysosomes were readily identified in HeLa cells, which we refer to as dense tubular, multilamellar, and multivesicular structures (Figure 4). Multivesicular endosomes contained one or more internal vesicles, multilamellar endosomes/lysosomes contained concentric layers of membranes or membrane whorls, and dense tubular endosomes/lysosomes contained a dense network of internal membranes and may represent the MPR-enriched late endosomes described by Griffiths *et al*. (1988) (Figure 4A, left). These latter structures were either present as single entities or were found in larger, membrane-bound compartments in combination with one or more of the three structural types. Immunogold labeling further confirmed that each of these structural classes included late endosomes because both Rab7 (large gold) and Rab9 (small gold) could be detected on their surfaces (Figure 4B). Although not all Rab7 and Rab9 colocalize on individual late endosomes (Figure 2A, left), examples of structures containing both proteins were readily detected by immunoelectron microscopy (Figure 4B). It is important to note that most anti-Rab9 staining was seen on the multivesicular endosome class, which includes both early and late endosomes subtypes.

Late endosomes are concentrated close to the microtubule organizing center. This area was identified in sections of control and Rab9-depleted HeLa cells and the number of each late endosome structural class was quantified (Figure 4C). Multivesicular late endosome numbers remained unchanged in control and Rab9 depleted cells, with approximately four structures per 5 μm^2. This is perhaps not surprising because multivesicular endosomes are generated from early endosomes through the sequential action of the endosomal complex required for transport (ESCRT) complexes (Katzmann *et al*., 2001; Babst *et al*., 2002a, 2002b). Thus, most of these structures are likely to represent predominantly, endosomes located earlier in the endocytic pathway than those that contain Rab9.

Dense tubular and multilamellar late endosomes/lysosomes were less common than multivesicular endosomes in a given section, averaging only one to two structures per 5 μm^2 in the perinuclear region of control cells (Figure 4C). Surprisingly, we found a clear reduction in the number of both of these structural classes in Rab9-depleted cells, with less than one structure identified per 5 μm^2 (Figure 4C). Therefore, Rab9 depletion influences the maintenance or generation of the dense tubular and especially, multilamellar structures. In addition to these subsets of endosome/lysosome compartments, essentially all kinetically defined late endosomes labeled in Figure 3 were reduced in size. It is important to note that most of the endosomes labeled in Figure 3 are likely not multilamellar or dense tubular structures, despite their decrease in size upon Rab9 depletion. This conclusion stems from our finding that most late endo-

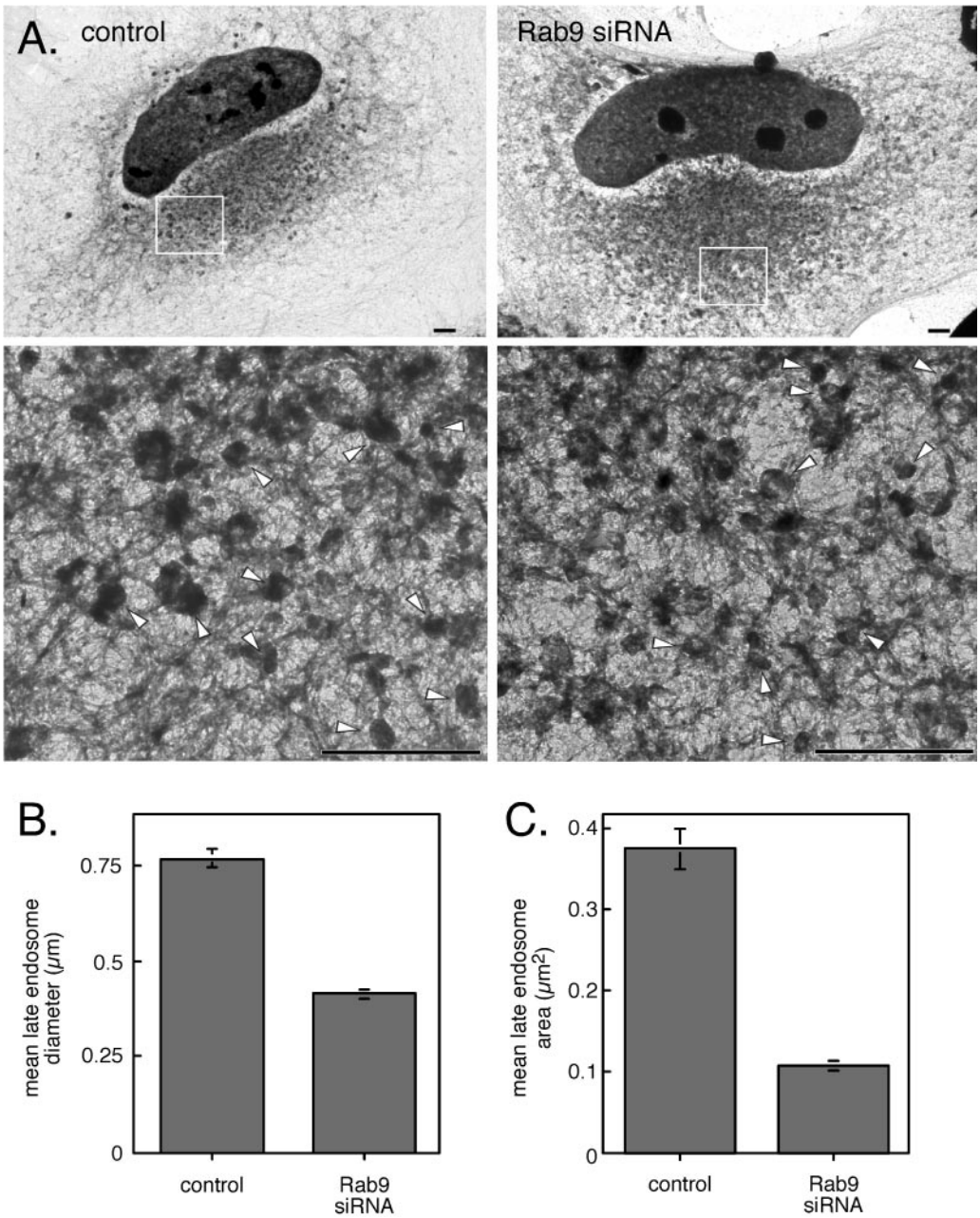

Figure 3. Rab9 depletion decreases late endosome size. (A) HeLa cells transfected with control siRNA (left) or Rab9 siRNA (right) were labeled by fluid phase endocytosis of HRP for 1 h at 37°C followed by a 30-min chase. Cells were then processed for whole-mount EM. The boxed regions in the top panels are shown magnified in the panels below and late endosomal structures are indicated with arrow heads. Bar, 2 μm. (B) Average diameter (left) and area (right) of 265 late endosomal structures from 14 different control siRNA-transfected cells and 248 late endosomal structures from 13 different Rab9 siRNA-transfected cells were measured. Results are from two independent experiments; error bars represent SE of the mean.

somal Rab9 is detected on multivesicular endosomes by immunoelectron microscopy.

How might Rab9 depletion decrease endosome size? In control-treated HeLa cells, prenylated Rab9 may be accommodated in membranes by an increase in late endosome membrane surface. Alternatively, Rab9 may play a role in the generation and/or maintenance of a larger subclass of late endosomes/lysosomes; in the absence of Rab9 these structures might fail to form or have a shorter lifetime. Because Rab9 is essential for the delivery of newly synthesized lysosomal enzymes to lysosomes, perhaps the loss of dense tubular and multilamellar structures simply reflects a primary defect in lysosome formation.

Biochemical Characterization of Dense Lysosomes

Electron micrographic analysis revealed a decrease in late endosome size in cells depleted of Rab9 protein (Figure 3). In addition, we noted a decrease in the number of dense tubular and especially multilamellar endocytic structures (Figure 4). Although most Rab9 was normally present on multive-

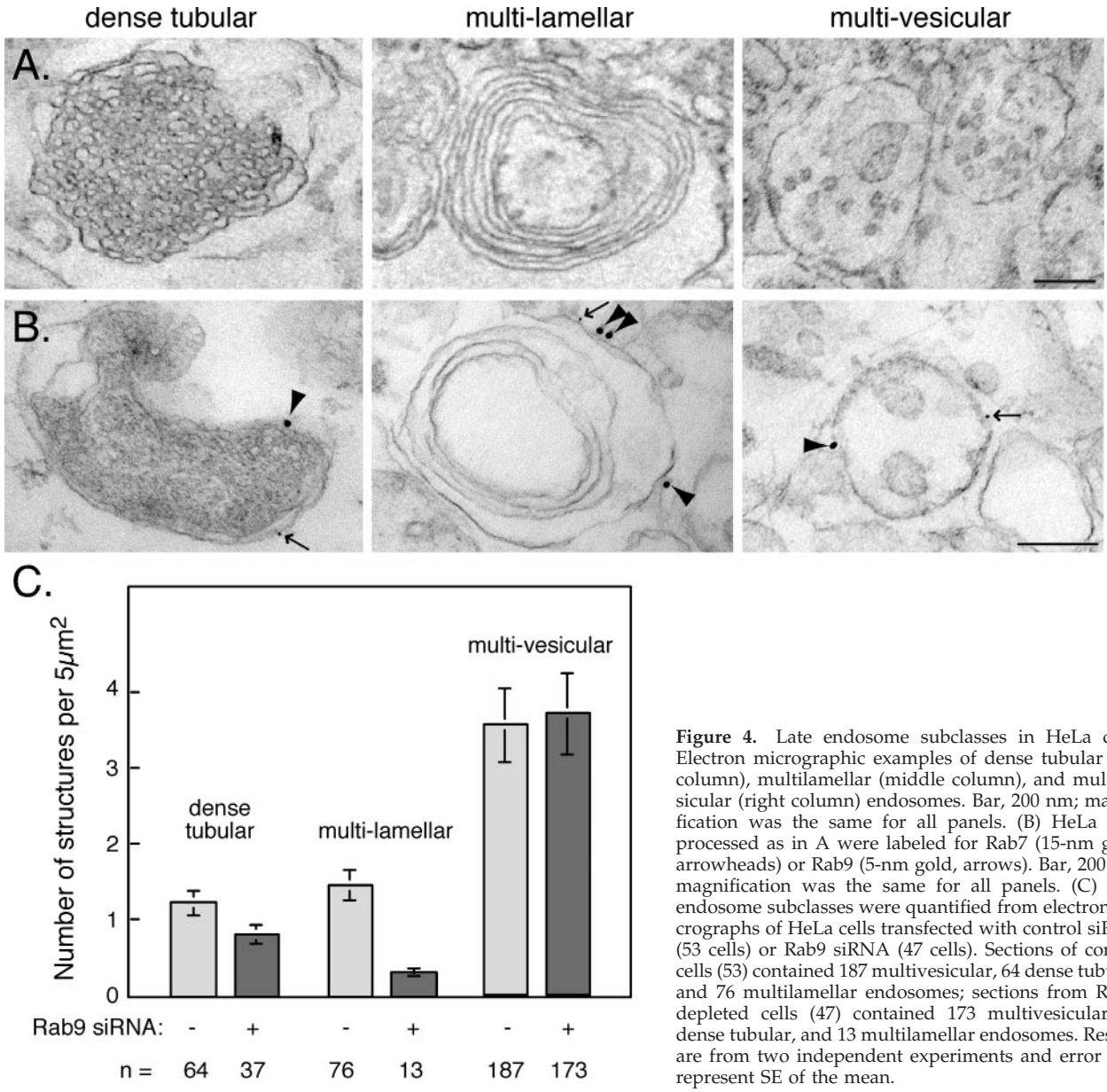

Figure 4. Late endosome subclasses in HeLa cells. Electron micrographic examples of dense tubular (left column), multilamellar (middle column), and multivesicular (right column) endosomes. Bar, 200 nm; magnification was the same for all panels. (B) HeLa cells processed as in A were labeled for Rab7 (15-nm gold, arrowheads) or Rab9 (5-nm gold, arrows). Bar, 200 nm; magnification was the same for all panels. (C) Late endosome subclasses were quantified from electron micrographs of HeLa cells transfected with control siRNA (53 cells) or Rab9 siRNA (47 cells). Sections of control cells (53) contained 187 multivesicular, 64 dense tubular, and 76 multilamellar endosomes; sections from Rab9-depleted cells (47) contained 173 multivesicular, 37 dense tubular, and 13 multilamellar endosomes. Results are from two independent experiments and error bars represent SE of the mean.

sicular late endosomes, it was important to evaluate the overall status of the lysosome compartment in Rab9-depleted cells because it was possible that the multilamellar structures were lysosomal in origin. Also, as seen previously (Riederer *et al*., 1994), lysosomal enzyme levels were upregulated to compensate for the loss of Rab9 protein: LAMP1 protein and hexosaminidase activity were increased by 58 and 56%, respectively, in Rab9-depleted cells (Figure 1A; our unpublished data). Thus, we used a procedure devised by Kornfeld and colleagues for rapid separation of dense lysosomes, which are collected in the lower 30% (fraction 3) of a Percoll gradient (Rohrer *et al*., 1995).

As expected, the bulk of the lysosomal LAMP1 protein was recovered in fraction 3 (Figure 5, bottom). In addition, despite slight increases in lysosomal enzymes, the relative amounts of protein (Figure 5, top), phospholipid (middle), and LAMP1 protein (bottom) were not significantly different when Rab9-depleted and control cells were compared. Therefore, lysosomal enzyme activity per mole phospholipid or protein did not change relative to other membrane-bound compartments as determined by this global biochemical analysis.

Although late endosomes decreased in size (Figure 3), the buoyant densities of markers that are in part present in late endosomes (hexosaminidase [our unpublished data] and LAMP1) were generally unchanged. In summary, these fractionation experiments lead us to conclude that the decrease in multilamellar structures (Figure 4) does not significantly influence the overall distribution of enzymes among late endosomes and lysosomes.

Rab9 Influences Trafficking of Other Late Endosome Markers

As shown in Figure 1, the loss of Rab9 protein led to an increase in total cellular CI-MPR coupled with an enhancement in the rate of this protein's degradation. In addition, we noted that cells contained higher levels of surface MPRs

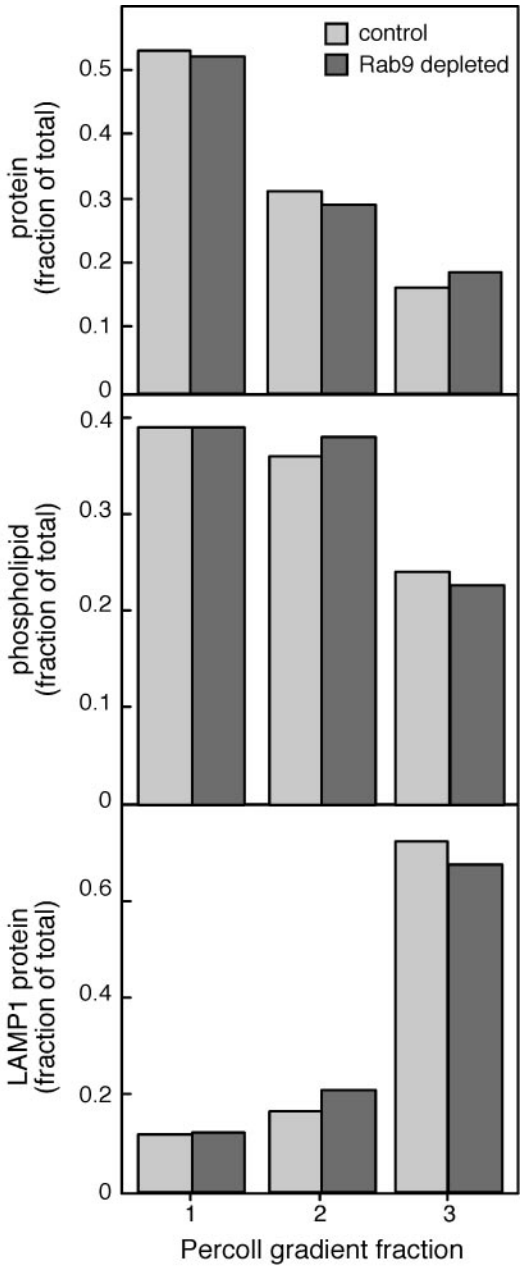

Figure 5. Percoll density gradient analysis of Rab9-depleted cell membranes. Control and Rab9-depleted cells were harvested and fractionated as described by Rohrer *et al*. (1995); the gradients were divided into three fractions and analyzed for protein (top), phospholipid (middle), and LAMP1 protein (bottom). All data are presented as fraction of total.

and early endosome MPRs. This was easily detected in experiments in which cells were incubated with anti-MPR antibodies for short periods of time (15 min; Figure 6). Under these conditions, Rab9-depleted cells internalized significantly more antibody than control cells (Figure 6, top). In addition, these cells internalized increased amounts of LAMP1 antibody (Figure 6, bottom). Although some of the increase of cell surface MPRs may be due to an increase in their biosynthesis, LAMP1 protein levels were only increased by 58% upon Rab9 depletion (Figure 1). Thus, it seems that Rab9 contributes to the retention of a fraction of MPRs and LAMP1 within late endosomes, either via microdomain incorporation or by regulation of endosome egress. In the absence of Rab9 protein, endosome-to-cell surface transport seems to be enhanced. The presence of LAMP1 on the surface is consistent with an essential role for Rab9 in early events of lysosome formation.

Rab9 Stability Requires Effector Interaction

As described above, endosome-associated Rab9 recruits its cytosolic effector protein, TIP47, which binds to MPR cytoplasmic domains (Diaz and Pfeffer, 1998; Carroll *et al*., 2001). TIP47 binding is thought to enrich MPRs within a Rab9 microdomain and thereby facilitate MPR collection into nascent transport vesicles. We investigated TIP47's role in stabilizing this microdomain by using siRNA to deplete TIP47 from cultured cells. Immunoblot and immunofluorescence analysis showed that TIP47 levels could be decreased up to 80% by siRNA treatment (Figure 7, A and B). In the presence of TIP47 siRNA, but not a control lamin A/C siRNA, TIP47 protein levels decreased with time of treatment (our unpublished data). Steady-state levels of Rab9, Rab7, LAMP1 protein (Figure 7A), and CI-MPR (our unpublished data) did not change substantively upon depletion of TIP47. Moreover, immunofluorescence microscopy detected Rab9 on what seemed to be normal, perinuclear, late endosomal structures (our unpublished data).

The apparent minimal changes in the steady-state levels and localizations of MPRs and Rab9 proteins masked significant changes in protein stability as determined by pulse chase labeling of the proteins and examination of their turnover (Figure 7C). In previous work, antisense depletion to reduce TIP47 protein levels by ~50% led to MPR missorting to the lysosome and it reduced the CI-MPR half-life by twofold (Diaz and Pfeffer, 1998). Thus, as expected, TIP47 siRNA decreased the stability of CI-MPR 1.9-fold, reducing the protein half-life from 26 to 14 h (Figure 7C). The change in turnover was not due to a general increase in protein turnover because the low-density lipoprotein receptor lifetime was unchanged (Figure 7C). Unexpectedly, the half-life of Rab9 protein decreased from 32 to 8 h, a fourfold decrease in stability due to loss of TIP47. The effect was specific for Rab9 because the half-life of Rab7 protein was completely unchanged (Figure 7C).

The apparent minimal change in the steady-state level of Rab9 protein, coupled with a greatly increased rate of degradation, suggests that Rab9 gene expression is induced upon TIP47 depletion. How TIP47 depletion triggers Rab9 transcription is unknown. As was observed for Rab9 depletion (Figure 1C), EGF-stimulated EGF receptor degradation was unchanged in TIP47-depleted cells, suggesting that overall late endosome function was retained (our unpublished data).

Why should Rab9 protein be much more rapidly degraded in the absence of TIP47? Investigators in this research area generally think of prenylated Rabs as either existing in the outer leaflet of an organelle membrane or bound to the carrier protein GDP dissociation inhibitor (GDI) in the cytosol. Prenylated Rabs are considered independent entities, despite their ability to interact with a variety of important effector proteins (Zerial and McBride, 2001). Yet, when TIP47 was depleted from cells, Rab9 protein was rapidly degraded, either via proteosomal degradation or delivery to lysosomes. Thus, we cannot think of Rabs as truly independent constituents: their interactions with effectors can influence greatly, their cellular fates. In summary, TIP47 is essential for both Rab9 stabilization and MPR recycling. Together, these data support a model in which TIP47 interacts with

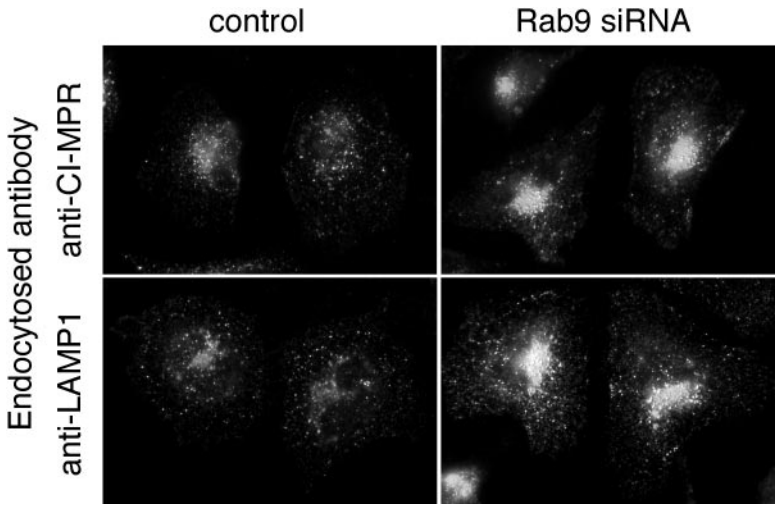

Figure 6. Loss of Rab9 increases cell surface CI-MPR and LAMP1. HeLa cells transfected with buffer alone (left) or Rab9 siRNA (right) were incubated with anti-CI-MPR antibody (top) or anti-LAMP1 antibody (bottom) for 15 min before extensive washing, fixing, and staining with fluorescent secondary antibody.

MPRs and Rab9 protein in living cells. Moreover, these data highlight the independent regulation of Rab9 and Rab7 endosomal domains because Rab7 protein was not destabilized upon loss of Rab9 or TIP47 proteins.

Stabilization of the Rab9 Microdomain in Living Cells

Prenylated Rab proteins are delivered to membranes by GDI and are thought to be in equilibrium between membranes and a cytosolic, GDI-bound form. We have shown that in the absence of TIP47, Rab9 protein is significantly destabilized. One possibility is that Rab9 membrane association is normally favored by TIP47 binding, relative to GDI-mediated, membrane release. If true, TIP47 depletion might increase the amount of cytosolic Rab9. As shown in Figure 8A, we detected a twofold increase in the level of cytosolic Rab9 upon TIP47 depletion. Although ~10% of total Rab9 was found bound to GDI in control cell cytosol, depletion of TIP47 increased that value to 20% (Figure 8A). We cannot completely exclude the possibility that this increase reflects an increase in newly synthesized Rab9 protein en route to endosomes. Newly synthesized Rab proteins are believed to be delivered to membranes by the Rab escort protein (Alexandrov *et al*., 1994), but GDI also may play a role (Sanford *et al*., 1995). Nevertheless, the absence of TIP47 seems to shift the equilibrium between membrane-associated and cytosolic Rab9 protein.

Given the importance of TIP47 for Rab9 stabilization on endosomes, we determined the affinity of interaction between these binding partners. For this purpose we made use of the fact that the presence of TIP47 in Rab9 nucleotide binding assays leads to a higher level of overall nucleotide binding (Hanna *et al*., 2002). This method could thus be used as an indirect measure of physical interaction. An advantage of this approach is that it detects only active Rab9 protein binding to TIP47, and it uses binding of radiolabeled nucleotide to determine quantitatively, the amount of Rab9-bound TIP47 protein.

As shown in Figure 8B, the affinity of TIP47 for Rab9 bound to GTPγS was strong (K_d = 95 nM; filled circles). The affinity of TIP47 for Rab9 bound to GDP was lower (K_d = 160 nM; open circles). Thus, the interaction between TIP47 and Rab9 is of high affinity—almost 10-fold higher than the affinity of TIP47 for the cytoplasmic domain of the MPR (K_d = 1 μM; Krise *et al*., 2000). The high affinity of TIP47 for Rab9 is consistent with the importance of this interaction in stabilizing Rab9 protein and supports a model in which Rab9 recruits TIP47 onto late endosomes.

DISCUSSION

Late endosomes represent an intermediate way-station for receptors and ligands en route to lysosomes. They also house a large fraction of mannose 6-phosphate receptors, which are retrieved from this compartment by Rab9 and TIP47 proteins. We have shown here that the morphology of late endosomes is significantly altered in cells depleted of Rab9. These cells displayed a reduction in late endosome size, as monitored by whole mount electron microscopy of HRP-labeled late endosomes. The reduction in late endosome size was unexpected: Rab9 is not an especially abundant protein, and by blocking the MPR retrieval pathway, Rab9 depletion might have instead led to the enlargement of the compartment. The shrinkage of late endosomes in Rab9-depleted cells suggests that other late endosome exit routes continue unabated to remove late endosome membrane constituents either toward the lysosome or toward the plasma membrane. Indeed, Rab9 depletion led to an increase in surface-localized LAMP1 protein.

Previous studies support the importance of Rabs for organelle size regulation. For example, overexpression of Rab5 enlarges early endosomes, whereas overexpression of a GDP-bound Rab5 mutant causes their fragmentation (Bucci *et al*., 1992; Stenmark *et al*., 1994; Wucherpfennig *et al*., 2003). In this example, the Rab mediates early endosomal, homotypic fusion, and the size change reflects Rab5's fusion-stimulating activity. It is not known whether Rab9 mediates an endosomal fusion event; Rab7 is believed to carry out this function on late endosomes (Feng *et al*., 1995; Vitelli *et al*., 1997). Whereas a decrease in endosome size seen on Rab9 depletion is consistent with a requirement for Rab9 in an endosome fusion event, no endosome enlargement was observed when wild-type Rab9 was overexpressed in our previous studies (Riederer *et al*., 1994). We favor an alternative explanation. There are many examples in the literature of membrane protein levels regulating the size and morphology of membrane compartments (Pfeffer, 2003). For example, the endoplasmic reticulum (ER) is exaggerated in cells that express enzymes of lipid biosynthesis, and overexpression of HMG CoA reductase generates an unusual, crystalloid ER (cf. Pfeffer, 2003). In normal late endosomes, Rab9

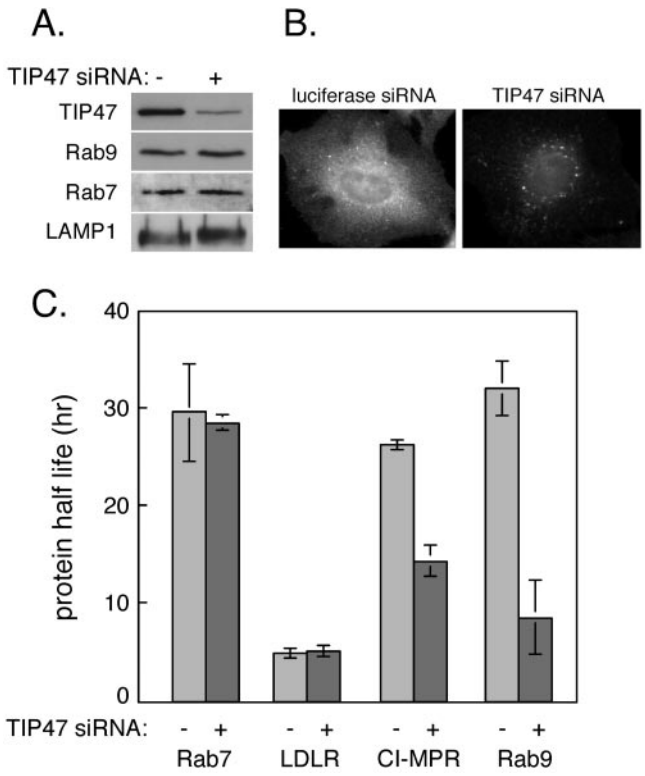

Figure 7. TIP47 is required for Rab9 and CI-MPR stability. (A) Immunoblot analysis of equal amounts of protein from HeLa cell lysates transfected with control siRNA (−) or TIP47 siRNA (+) were analyzed using the indicated antibodies. (B) Anti-TIP47 antibody indirect immunofluorescence of cells treated with control luciferase siRNA (left) or TIP47 siRNA (right). Note that certain spots are not lost upon TIP47 siRNA treatment. We believe these may represent lipid droplets that our antibody cross-reacts with (Barbero *et al.*, 2001). (C) [^{35}S]methionine/cysteine pulse-chase analysis of protein turnover in HeLa S3 cells transfected with control or TIP47 siRNA. Shown are the half-lives of the indicated proteins; values are the average from two independent experiments. Error bars represent SD.

may organize a complex microdomain of protein–protein and protein–lipid interactions that is disrupted in its absence.

The dense tubular structures that decreased in number upon Rab9 depletion may represent those characterized by Griffiths *et al*. (1988, 1990). These workers showed that the internal membranes of these prelysosomal compartments could be labeled extensively with anti-MPR antibodies. How these internal membranes form is entirely unclear. The complex internal membrane architecture may derive from multivesicular bodies generated at the early endosome through the action of the ESCRT machinery (Katzmann *et al*., 2001; Babst *et al*., 2002a,b). Depletion of Hrs, a protein involved in ESCRT recruitment to early endosomes, resulted in large, late endosomal/lysosomal structures that were devoid of internal membranes (Bache *et al*., 2003). Likewise, depletion of the protein Alix, which also interacts with ESCRT proteins, caused a reduction in the number of multilamellar late endosomes (Matsuo *et al*., 2004). Because loss of Rab9 destabilized MPRs and likely also the TIP47-organized, late endosome microdomain, perhaps this set of interactions is required for the generation and/or maintenance of multilamellar and dense tubular endosomes.

A final possibility is that upon Rab9 depletion, lysosomal hydrolases are significantly induced to compensate for MPR-trafficking defects and missorting. In the presence of additional hydrolytic activity, the internal membranes of multilamellar and dense tubular endosomes might be more rapidly degraded, leading to the disappearance of the compartments. It is important to note that LAMP1 and hexosaminidase were only slightly induced in Rab9-depleted cells, similar to our previous studies, in which cells stably expressing a dominant negative Rab9 protein showed only a 60% increase in cathepsin D and hexosaminidase and a twofold increase in β-glucuronidase activity (Riederer *et al*., 1994). Although we cannot rule out this model, it seems unlikely that a minor change in enzyme levels would be adequate to remove an entire class of endosomes within 72 h after siRNA transfection.

Similar to cells expressing a Rab9 dominant negative mutant protein (Riederer *et al*., 1994), Rab9-depleted cells showed somewhat elevated levels of surface MPRs and early endosomal MPRs. This may be a consequence of the increase in new MPR biosynthesis, coupled with endosome destabilization and increased degradation. These two events would together decrease the steady-state level of MPRs in late endosomes.

The increase in surface LAMP1 protein was not expected and suggests that endosome to plasma membrane transport is enhanced in these cells (Lippincott-Schwartz and Fambrough, 1987). A similar missorting is seen in fibroblasts from Hermansky-Pudlak patients that have reduced levels of the cargo adaptor AP-3. In these cells, LAMP proteins show increased cycling to the cell surface, despite a steady-state, perinuclear localization (Dell'Angelica *et al*., 1999, 2000).

We did not expect that Rab9 would require TIP47 for its stability on late endosomes. Models of Rab GTPases depict them as prenylated membrane constituents, cycling merrily between the cytosol and membrane surfaces. Very little is known about what targets Rab proteins for degradation. The results presented here show for the first time that an effector interaction is essential for Rab stability. Although a half-life of 8 h may seem long for a protein that might be carried to the *trans*-Golgi network many times before its destruction, this must be contrasted with a normal half-life for Rab9 of ~30 h. The dynamics of membrane microdomain assembly and stabilization will be important to analyze further. Unfortunately, our attempts to distinguish the pathway of Rab9 degradation by using inhibitors of cytoplasmic or lysosomal degradation were inconclusive; the long half-life of Rab9 required that cells be treated with inhibitors for times longer than they could healthily withstand.

TIP47 depletion destabilized both Rab9 and CI-MPRs, but not Rab7. Although a significant fraction of Rab9-containing compartments contain Rab7, loss of Rab9 had no effect on the steady-state level or turnover of Rab7. This suggests that the Rab9 microdomain is regulated independently of neighboring Rab7 protein and presumably Rab7-interacting proteins.

In summary, Rab9 contributes either directly or indirectly to the generation and/or maintenance of specific morphological classes of late endocytic compartments. Rab9 influences the size of late endosomes. In addition, TIP47 is key to the stability of Rab9 and other proteins contained within the late endosomal, Rab9 microdomain. How these proteins act to regulate endosome morphology and localization will be important areas for future investigation.

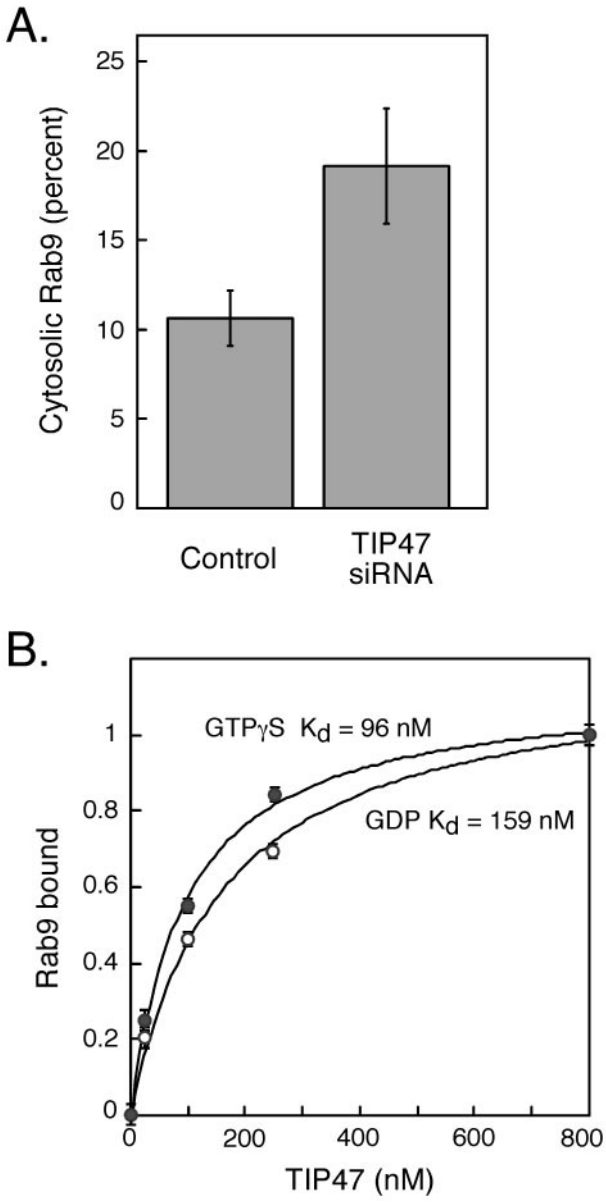

Figure 8. Rab9 binds TIP47 with high affinity and shifts to the cytosol upon TIP47 depletion. (A) Equal amounts of crude cytosol and membrane fractions from control and TIP47 siRNA-transfected HeLa cells were analyzed by immunoblotting with anti-Rab9 antibodies. Duplicate blots from two independent experiments were quantified. Shown is the average percentage of total cellular Rab9 in the cytosol of control and TIP47-depleted cells. Error bars represent SD. (B) Binding affinity of Rab9 and TIP47. The lines represent theoretical curve fits to experimental data according to the equation describing bimolecular reversible binding. Estimates for K_d were generated using a curve-fitting algorithm (Kaleidagraph). Fraction of Rab9 binding to TIP47 was normalized to between 0 and 1; data shown are the average of two separate experiments. Rab9-GTPγS, closed circles; Rab9-GDP, open circles.

ACKNOWLEDGMENTS

We thank John Perrino (Stanford University Medical Center's Cell Sciences Imaging Facility) for help with processing EM samples and members of the Pfeffer laboratory for critical comments. This research was funded by a grant from the National Institutes of Health (DK-37332).

REFERENCES

Alexandrov, K., Horiuchi, H., Steele-Mortimer, O., Seabra, M.C., and Zerial, M. (1994). Rab escort protein-1 is a multifunctional protein that accompanies newly prenylated rab proteins to their target membranes. EMBO J. *13*, 5262–5273.

Babst, M., Katzmann, D.J., Estepa-Sabal, E.J., Meerloo, T., and Emr, S.D. (2002a). Escrt-III: an endosome-associated heterooligomeric protein complex required for MVB sorting. Dev. Cell *3*, 271–282.

Babst, M., Katzmann, D.J., Snyder, W.B., Wendland, B., and Emr, S.D. (2002b). Endosome-associated complex, ESCRT-II, recruits transport machinery for protein sorting at the multi-vesicular body. Dev. Cell *3*, 283–289.

Bache, K.G., Brech, A., Mehlum, A., and Stenmark, H. (2003). Hrs regulates multi-vesicular body formation via ESCRT recruitment to endosomes. J. Cell Biol. *162*, 435–442.

Barbero, P., Buell, E., Zulley, S., and Pfeffer, S.R. (2001). TIP47 is not a component of lipid droplets. J. Biol. Chem. *276*, 24348–24351.

Barbero, P., Bittova, L., and Pfeffer, S.R. (2002). Visualization of Rab9-mediated vesicle transport from endosomes to the trans-Golgi in living cells. J. Cell Biol. *156*, 511–518.

Bucci, C., Parton, R.G., Mather, I.H., Stunnenberg, H., Simons, K., Hoflack, B., and Zerial, M. (1992). The small GTPase rab5 functions as a regulatory factor in the early endocytic pathway. Cell *70*, 715–728.

Carroll, K.S., Hanna, J., Simon, I., Krise, J., Barbero, P., and Pfeffer, S.R. (2001). Role of Rab9 GTPase in facilitating receptor recruitment by TIP47. Science *292*, 1373–1376.

Dell'Angelica, E.C., Aguilar, R.C., Wolins, N., Hazelwood, S., Gahl, W.A., and Bonifacino, J.S. (2000). Molecular characterization of the protein encoded by the Hermansky-Pudlak syndrome type 1 gene. J. Biol. Chem. *275*, 1300–1306.

Dell'Angelica, E.C., Shotelersuk, V., Aguilar, R.C., Gahl, W.A., and Bonifacino, J.S. (1999). Altered trafficking of lysosomal proteins in Hermansky-Pudlak syndrome due to mutations in the beta 3A subunit of the AP-3 adaptor. Mol. Cell *3*, 11–21.

Diaz, E., and Pfeffer, S.R. (1998). TIP47: a cargo selection device for mannose 6-phosphate receptor trafficking. Cell *93*, 433–443.

Diaz, E., Schimmoller, F., and Pfeffer, S.R. (1997). A novel Rab9 effector required for endosome-to-TGN transport. J. Cell Biol. *138*, 283–290.

Dintzis, S.M., Velculescu, V.E., and Pfeffer, S.R. (1994). Receptor extracellular domains may contain trafficking information. Studies of the 300-kDa mannose 6-phosphate receptor. J. Biol. Chem. *269*, 12159–12166.

Elbashir, S.M., Harborth, J., Lendeckel, W., Yalcin, A., Weber, K., and Tuschl, T. (2001). Duplexes of 21-nucleotide RNAs mediate RNA interference in cultured mammalian cells. Nature *411*, 494–498.

Feng, Y., Press, B., and Wandinger Ness, A.)1995). Rab7: an important regulator of late endocyutic membrane traffic. J. Cell Biol. *131*, 1435–1452.

Griffiths, G., Hoflack, B., Simons, K., Mellman, I., and Kornfeld, S. (1988). The mannose 6-phosphate receptor and the biogenesis of lysosomes. Cell *52*, 329–341.

Griffiths, G., Matteoni, R., Back, R., and Hoflack, B. (1990). Characterization of the cation-independent mannose 6-phosphate receptor-enriched prelysosomal compartment in NRK cells. J. Cell Sci. *95*, 441–461.

Hanna, J., Carroll, K., and Pfeffer, S.R. (2002). Identification of residues in TIP47 essential for Rab9 binding. Proc. Natl. Acad. Sci. USA *99*, 7450–7454.

Itin, C., Rancano, C., Nakajima, Y., and Pfeffer, S.R. (1997). A novel assay reveals a role for soluble N-ethylmaleimide-sensitive fusion attachment protein in mannose 6-phosphate receptor transport from endosomes to the trans Golgi network. J. Biol. Chem. *272*, 27737–27744.

Itin, C., Ulitzur, N., Muhlbauer, B., and Pfeffer, S.R. (1999). Mapmodulin, cytoplasmic dynein, and microtubules enhance the transport of mannose 6-phosphate receptors from endosomes to the trans-Golgi network. Mol. Biol. Cell *10*, 2191–2197.

Katzmann, D.J., Babst, M., and Emr, S.D. (2001). Ubiquitin-dependent sorting into the multi-vesicular body pathway requires the function of a conserved endosomal protein sorting complex, ESCRT-I. Cell *106*, 145–155.

Kleijmeer, M., *et al*. (2001). Reorganization of multi-vesicular bodies regulates M.H.C. class II antigen presentation by dendritic cells. J. Cell Biol. *155*, 53–63.

Kornfeld, S. (1992). Structure and function of the mannose 6-phosphate/insulinlike growth factor II receptors. Annu. Rev. Biochem. *61*, 307–330.

Krise, J.P., Sincock, P.M., Orsel, J.G., and Pfeffer, S.R. (2000). Quantitative analysis of TIP47-receptor cytoplasmic domain interactions: implications for endosome-to-trans Golgi network trafficking. J. Biol. Chem. *275*, 25188–25193.

Lippincott-Schwartz, J., and Fambrough, D.M. (1987). Cycling of the integral membrane glycoprotein, LEP100, between plasma membrane and lysosomes: kinetic and morphological analysis. Cell *49*, 669–677.

Lombardi, D., Soldati, T., Riederer, M.A., Goda, Y., Zerial, M., and Pfeffer, S.R. (1993). Rab9 functions in transport between late endosomes and the trans Golgi network. EMBO J. *12*, 677–682.

Matsuo, H., *et al*. (2004). Role of LBPA and Alix in multivesicular liposome formation and endosome organization. Science *303*, 531–534.

Miaczynska, M., and Zerial, M. (2002). Mosaic organization of the endocytic pathway. Exp. Cell Res. *272*, 8–14.

Orsel, J.G., Sincock, P.M., Krise, J.P., and Pfeffer, S.R. (2000). Recognition of the 300-kDa mannose 6-phosphate receptor cytoplasmic domain by 47-kDa tail-interacting protein. Proc. Natl. Acad. Sci. USA *97*, 9047–9051.

Pfeffer, S. (2003). Membrane domains in the secretory and endocytic pathways. Cell *112*, 507–517.

Riederer, M.A., Soldati, T., Shapiro, A.D., Lin, J., and Pfeffer, S.R. (1994). Lysosome biogenesis requires Rab9 function and receptor recycling from endosomes to the trans-Golgi network. J. Cell Biol. *125*, 573–582.

Rohrer, J., Schweizer, A., Johnson, K.F., and Kornfeld, S. (1995). A determinant in the cytoplasmic tail of the cation-dependent mannose 6-phosphate receptor prevents trafficking to lysosomes. J. Cell Biol. *130*, 1297–1306.

Sanford, J.C., Yu, J., Pan, J.Y., and Wessling-Resnick, M. (1995). GDP dissociation inhibitor serves as a cytosolic acceptor for newly synthesized and prenylated Rab5. J. Biol. Chem. *270*, 26904–26909.

Seaman, M.N. (2004). Cargo-selective endosomal sorting for retrieval to the Golgi requires retromer. J. Cell Biol. *165*, 111–122.

Shapiro, A.D., Riederer, M.A., and Pfeffer, S.R. (1993). Biochemical analysis of rab9, a ras-like GTPase involved in protein transport from late endosomes to the trans Golgi network. J. Biol. Chem. *268*, 6925–6931.

Soldati, T., Rancano, C., Geissler, H., and Pfeffer, S.R. (1995). Rab7 and Rab9 are recruited onto late endosomes by biochemically distinguishable processes. J. Biol. Chem. *270*, 25541–25548.

Soldati, T., Riederer, M.A., and Pfeffer, S.R. (1993). Rab GDI: a solubilizing and recycling factor for rab9 protein. Mol. Biol. Cell *4*, 425–434.

Sonnichsen, B., De Renzis, S., Nielsen, E., Rietdorf, J., and Zerial, M. (2000). Distinct membrane domains on endosomes in the recycling pathway visualized by multicolor imaging of Rab4, Rab5, and Rab11. J. Cell Biol. *149*, 901–914.

Stenmark, H., Parton, R.G., Steele-Mortimer, O., Lutcke, A., Gruenberg, J., and Zerial, M. (1994). Inhibition of rab5 GTPase activity stimulates membrane fusion in endocytosis. EMBO J. *13*, 1287–1296.

Vitelli, R., Santillo, M., Lattero, D., Chiariello, M., Bifulco, M., Bruni, C.B., and Bucci, C. (1997). Role of the small GTPase Rab7 in the late endocytic pathway. J. Biol. Chem. *272*, 4391–4397.

Wucherpfennig, T., Wilsch-Brauninger, M., and Gonzalez-Gaitan, M. (2003). Role of Drosophila Rab5 during endosomal trafficking at the synapse and evoked neurotransmitter release. J. Cell Biol. *161*, 609–624.

Zerial, M., and McBride, H. (2001). Rab proteins as membrane organizers. Nat Rev Mol. Cell. Biol. *2*, 107–117.